



OPEN

SUBJECT AREAS:

ION CHANNELS IN THE
NERVOUS SYSTEM

CELLULAR NEUROSCIENCE

Received

19 August 2013

Accepted

30 January 2014

Published

13 February 2014

Correspondence and
requests for materials
should be addressed to
M.W.S. (mike.salter@
utoronto.ca)

* Current address:

Department of
Neuroscience,
Carleton University,
Ottawa, ON, Canada.

GluN2B and GluN2D NMDARs dominate synaptic responses in the adult spinal cord

Michael E. Hildebrand^{1,2*}, Graham M. Pitcher^{1,2}, Erika K. Harding^{1,2}, Hongbin Li^{1,2}, Simon Beggs^{1,2}
& Michael W. Salter^{1,2}

¹Program in Neurosciences & Mental Health, Hospital for Sick Children, Toronto, ON, Canada, ²Department of Physiology, University of Toronto, Toronto, ON, Canada.

The composition of the postsynaptic ionotropic receptors that receive presynaptically released transmitter is critical not only for transducing and integrating electrical signals but also for coordinating downstream biochemical signaling pathways. At glutamatergic synapses in the adult CNS an overwhelming body of evidence indicates that the NMDA receptor (NMDAR) component of synaptic responses is dominated by NMDARs containing the GluN2A subunit, while NMDARs containing GluN2B, GluN2C, or GluN2D play minor roles in synaptic transmission. Here, we discovered NMDAR-mediated synaptic responses with characteristics not described elsewhere in the adult CNS. We found that GluN2A-containing receptors contribute little to synaptic NMDAR responses while GluN2B dominates at synapses of lamina I neurons in the adult spinal cord. In addition, we provide evidence for a GluN2D-mediated synaptic NMDAR component in adult lamina I neurons. Strikingly, the charge transfer mediated by GluN2D far exceeds that of GluN2A and is comparable to that of GluN2B. Lamina I forms a distinct output pathway from the spinal pain processing network to the pain networks in the brain. The GluN2D-mediated synaptic responses we have discovered in lamina I neurons provide the molecular underpinning for slow, prolonged and feedforward amplification that is a fundamental characteristic of pain.

N-methyl-D-aspartate receptors (NMDARs) are a prominent subtype of ionotropic glutamate receptor¹, critical for physiological synaptic plasticity in the developing and mature CNS, and for aberrant plasticity and neuronal death in pathological disorders². The NMDAR is a multiprotein complex, the core of which is a heterotetrameric assembly of two glycine-binding GluN1 subunits and two glutamate-binding GluN2 subunits. GluN1 is encoded by a single gene, *GRIN1*, whereas there are four GluN2-subunit-encoding genes, *GRIN2A–D*. Because NMDARs comprised of differing GluN2 subunits have distinctive functional properties and are hypothesized to have differing physiological and pathological roles^{1,3}, a major question has been to determine the specific GluN1/GluN2 subunit composition contributing to NMDAR-mediated transmission at a given synapse.

GluN2A has emerged as the principal subtype of GluN2 mediating synaptic NMDAR responses in the adult brain^{4–8}. By contrast, the contribution of NMDARs comprised of GluN2B to synaptic responses is less than that of receptors comprised of GluN2A throughout the adult brain, and at many synapses GluN2B contributes much less than does GluN2A. The GluN2B subunit is nevertheless well-expressed in the adult but primarily localized at extrasynaptic sites⁹. Conversely, during embryonic and early postnatal development synaptic GluN2B is more prominent than is GluN2A^{6,10,11}. GluN2C shows sparse expression in the adult brain, except for the cerebellum and olfactory bulb where GluN2C is highly expressed beginning in the second postnatal week^{10,12}. An enduring mystery has been that, in contrast to the other GluN2 subunits, synaptic NMDAR responses mediated by GluN2D are lacking in the adult brain⁹.

Here, while investigating glutamatergic synaptic responses of neurons in lamina I of the adult spinal dorsal horn we discovered NMDAR-mediated synaptic responses with characteristics not previously described elsewhere in the adult CNS. Lamina I neurons form a critical part of the nociceptive neuronal network in the dorsal horn which processes inputs from primary sensory afferents and transmits the resultant nociceptive signals to the brain^{13,14}. The nociceptive network in the dorsal horn is a highly interconnected matrix comprising monosynaptic inputs from primary afferents as well as polysynaptic and monosynaptic inputs from local circuit neurons^{15–17}. In order to properly characterize the responses from glutamatergic synapses directly on lamina I neurons it was necessary to avoid activating the nociceptive network because such network activation generates prolonged,

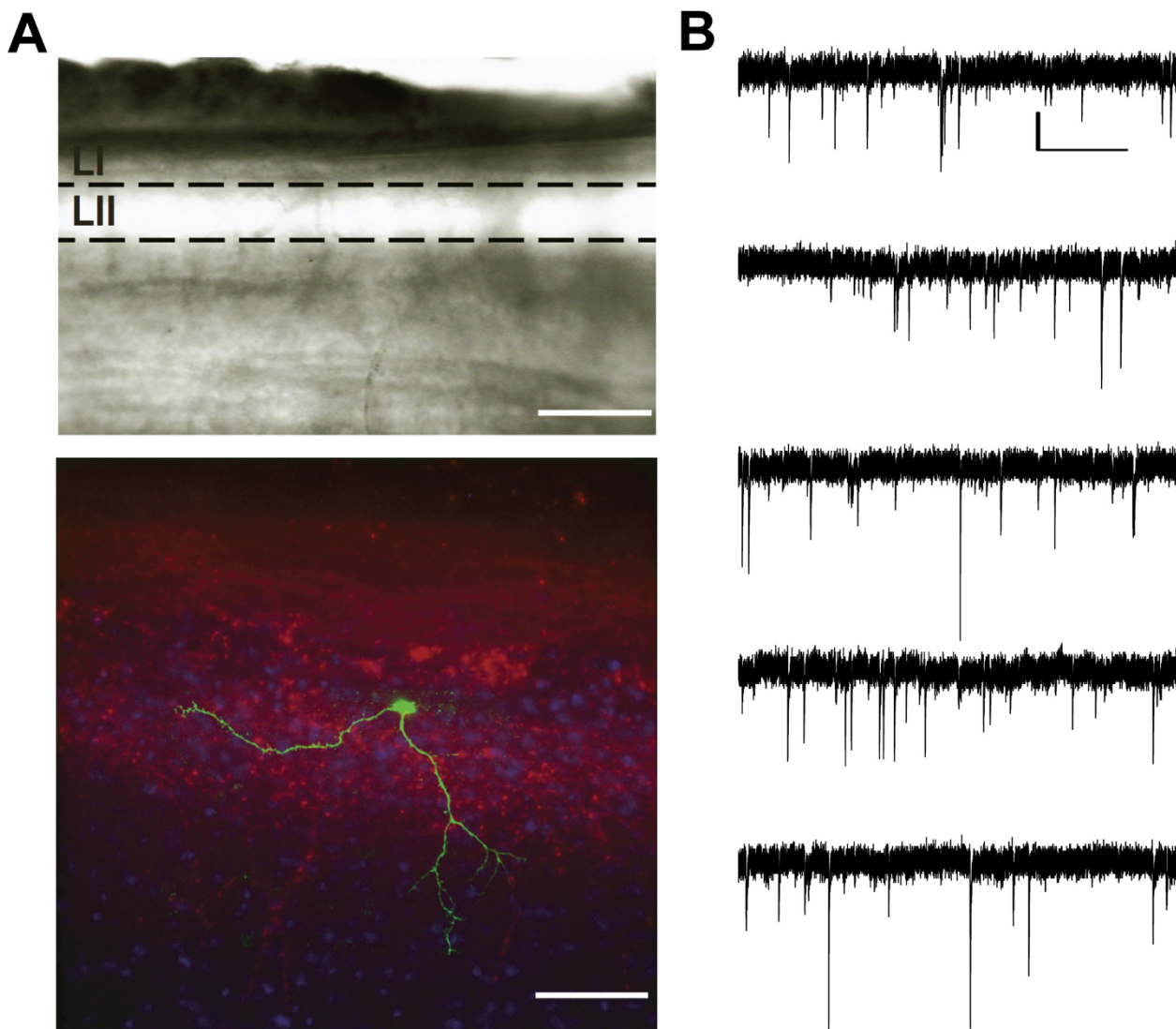


Figure 1 | Whole-cell patch recordings from lamina I neurons in rat parasagittal spinal cord slices. (A) *Top*, representative image of a parasagittal slice and micropipette during patch-clamp recording of a lamina I neuron. Through visual discrimination, the lamina I neuron was identified in the darker, striated, superficial-most layer of the dorsal horn (LI) compared to the more ventral, lighter substantia gelatinosa (LII), as indicated. Scale bar = 200 μm . *Bottom*, a two-photon image was taken from a lamina I neuron that was filled with lucifer yellow (0.1%, green) during whole-cell recording. Separately, an immunohistochemistry image was taken following slice fixation and staining for CGRP (red) and neuronal (NeuN, blue) labeling. The two-photon image was correctly scaled and superimposed onto the epifluorescence image stack to illustrate the location and orientation of the lamina I neuron within the superficial dorsal horn. Note neuronal morphology corresponding to a type Ib fusiform lamina I neuron⁶² as well as neuronal location within the outermost CGRP-stained dorsal horn region, characteristic of lamina I. Scale bar = 100 μm . (B) Raster plot of a representative continuous whole-cell recording from a lamina I neuron held at -60 mV. Scale bar x axis = 1 s, y axis = 10 pA.

largely polysynaptic excitatory responses which contaminate the direct NMDAR-mediated synaptic responses. To this end, in lamina I neurons we studied miniature excitatory postsynaptic currents (mEPSCs), representing the overall population of direct synaptic responses, and unitary primary afferent-evoked EPSCs, representing individual synapses. Surprisingly, we found that GluN2A contributes little to synaptic NMDAR responses while GluN2B dominates at lamina I synapses in adult spinal cord. Moreover, we discovered that there is a GluN2D-mediated synaptic NMDAR component of neurons in spinal lamina I and that the charge transfer mediated by GluN2D far exceeds that of GluN2A and is comparable to that of GluN2B.

Results

AMPA and NMDAR components of mEPSCs in lamina I neurons. We made whole-cell recordings from visually identified

lamina I neurons in acute, parasagittal slices of spinal cord from adult rats (see Methods; Fig. 1). All recordings were done in the presence of tetrodotoxin (TTX; 0.5 μM in ACSF) and cadmium (10 μM) to block action potential-dependent/ Ca^{2+} channel-dependent transmitter release. In addition, the recordings were done in the presence of bicuculline (10 μM) and strychnine (10 μM) to block GABA_A receptor- and glycine receptor-mediated responses, respectively. Under these conditions, in neurons held at -60 mV we observed spontaneously occurring inward currents (Fig. 1, 2A) that were blocked by the AMPA receptor (AMPA) antagonist, CNQX (10 μM ; not illustrated). Thus, the currents recorded were considered to be miniature excitatory post-synaptic currents (mEPSCs).

The average peak amplitude of the mEPSCs was -22 ± 1 pA ($n = 13$) and the average mEPSC frequency was 3.6 ± 0.9 Hz ($n = 13$) for lamina I neurons held at -60 mV. The distribution of mEPSC amplitudes showed a single peak around 20 pA and was skewed

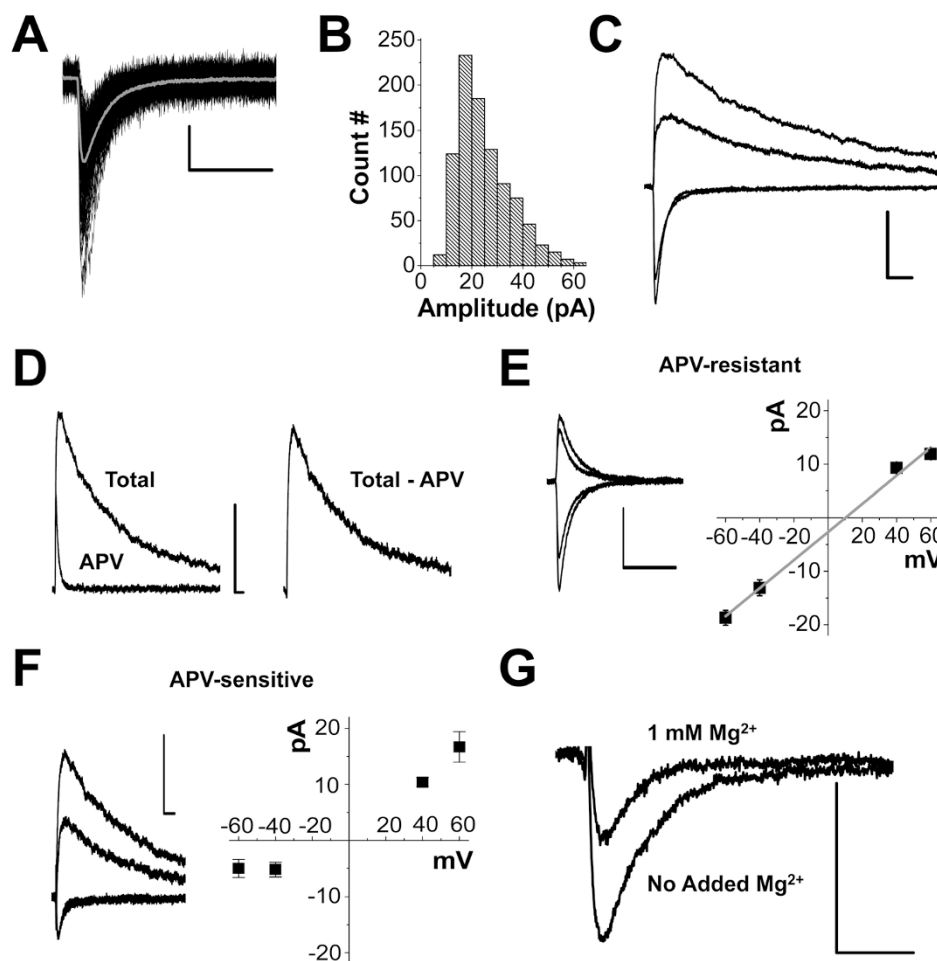


Figure 2 | Characterization of miniature excitatory postsynaptic currents (mEPSCs) in lamina I neurons from rat spinal cord slices. Whole-cell, voltage-clamp recordings of isolated spontaneous synaptic glutamatergic currents in ACSF including 500 nM TTX, 10 μ M bicuculline, 10 μ M strychnine, and 10 μ M Cd^{2+} . (A) Aligned individual mEPSCs at -60 mV for the cell shown in Figure 1B, with the averaged mEPSC trace shown in grey. (B) mEPSC peak amplitude histogram for lamina I neuronal recordings at -60 mV ($n = 13$ neurons). (C) Averaged mEPSC traces at -60 mV, -40 mV, $+40$ mV, and $+60$ mV ($n = 5$ neurons). (D) *Left*, averaged mEPSC traces at $+60$ mV in either the absence (“Total”, $n = 5$ neurons) or presence (“APV”, $n = 5$ neurons) of 100 μ M APV. *Right*, subtraction of the APV-resistant AMPAR-mEPSC component from the total mEPSC (from left) yields an NMDAR mEPSC component at $+60$ mV. (E) Averaged AMPAR mEPSC traces (100 μ M APV) at -60 mV, -40 mV, $+40$ mV and $+60$ mV (*left*) and associated current-voltage relationship (*right*) ($n = 5$). (F) *Left*, averaged NMDAR mEPSC traces at -60 mV, -40 mV, $+40$ mV, and $+60$ mV, derived from subtraction of mEPSCs in 100 μ M APV from control mEPSCs ($n = 5$), as in (D). *Right*, current-voltage relationships for NMDAR mEPSCs ($n = 5$). (G) Averaged NMDAR mEPSC traces at -60 mV with ($n = 5$) and without ($n = 5$) inclusion of 1 mM Mg^{2+} in the external solution. Scale bar x axes = 25 ms, y axes = 10 pA for all traces.

rightward (Fig. 2B), as is typical of mEPSCs recorded elsewhere in the mammalian CNS^{18,19}. At a holding potential of -60 mV the mEPSCs had a rapid rising phase (10–90% rise time = 1.2 ± 0.1 ms) and decayed with a time constant of 6.7 ± 0.5 ms ($n = 13$ cells). When lamina I neurons were held at positive membrane potentials ($+40$ or $+60$ mV) the mEPSCs rose rapidly but the decay phase was markedly longer than that of mEPSCs recorded at -60 mV (Fig. 2C). Administering the NMDAR antagonist, amino-phosphonovaleric acid (APV), abolished the slow decay of the mEPSCs recorded at positive holding potential (Fig. 2D). The residual APV-resistant component of the mEPSCs was blocked by CNQX, and had a time course that was symmetrical at negative and positive holding potentials. The current-voltage relationship of the APV-resistant mEPSC was linear (Fig. 2E) with the average conductance 0.26 ± 0.01 nS ($n = 5$). By contrast, the current-voltage relationship of the APV-sensitive component of the mEPSCs was outwardly-rectifying (Fig. 2F). Moreover, the APV-sensitive component recorded at -60 mV was robustly increased in neurons recorded without added extracellular Mg^{2+} (Fig. 2G). From these findings we conclude that mEPSCs in

lamina I neurons are dual component synaptic responses comprised of AMPAR-mediated and NMDAR-mediated components.

GluN2B dominates over GluN2A in mEPSCs in adult lamina I neurons. To investigate which subtypes of GluN2 mediate the NMDAR mEPSCs in adult lamina I neurons (Fig. 3), we utilized the distinctive pharmacological sensitivity and kinetic properties of NMDARs comprised of different GluN2s^{3,20}. Pharmacological sensitivity of the NMDARs mediating mEPSCs was assessed in neurons held at $+60$ mV; we measured the peak NMDAR currents and calculated the NMDAR-mediated charge transfer during a time period after the AMPAR component had fully decayed (40–500 ms after mEPSC onset). We tested for the involvement of GluN2A by using the GluN2A selective antagonist TCN-201²¹. We chose a concentration of TCN-201 (3 μ M) which is reported to inhibit NMDARs containing GluN2A by $\sim 90\%$ but which has no effect on those containing GluN2B, C or D²¹ (see Methods). The NMDAR component of mEPSCs recorded in the presence of TCN-201 (2.86 ± 0.25 pC; $n = 12$ neurons) was

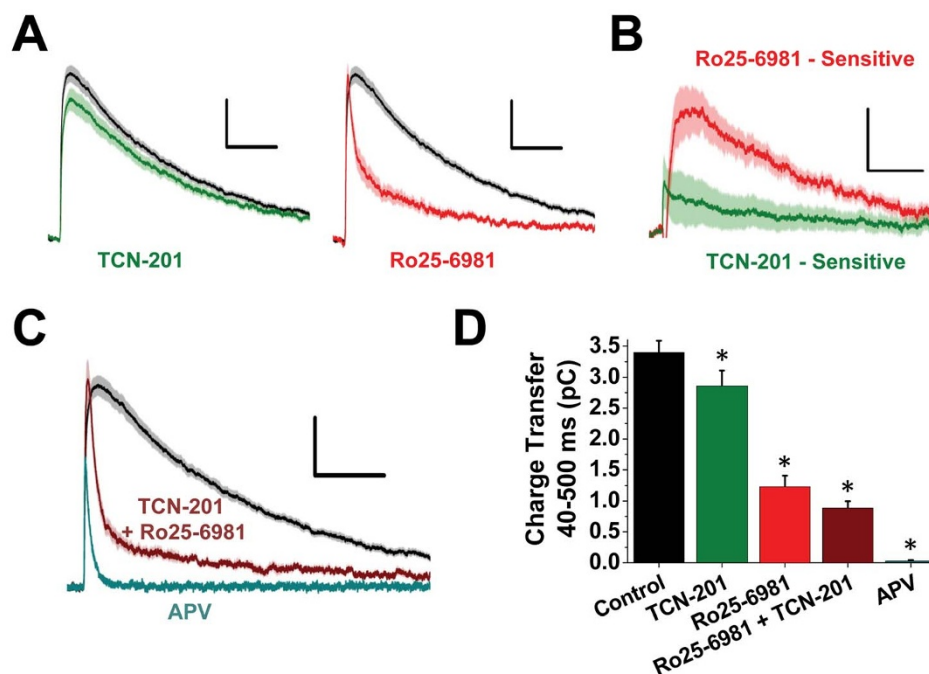


Figure 3 | Synaptic NMDAR currents are potently inhibited by Ro25-6981 and not TCN-201 in lamina I neurons of adult rats. (A) Average mEPSC traces at +60 mV in lamina I neurons treated with 3 μ M TCN-201 (*left*, green, $n = 12$) or 1 μ M Ro25-6981 (*right*, red, $n = 12$) compared to control mEPSC traces (black, $n = 24$). (B) Plots of +60 mV mEPSC subtraction traces based on data shown in (A), including control minus TCN treatment (green) and control minus Ro25-6981 treatment (red). (C) Average mEPSC traces at +60 mV including control-treated neurons (black, $n = 24$), neurons treated with 3 μ M TCN-201 and 1 μ M Ro25-6981 (maroon, $n = 7$), and neurons treated with 100 μ M APV (light blue, $n = 5$). (D) Histogram of NMDAR-mediated charge transfer (from 40 to 500 ms) measured from mEPSCs recorded at +60 mV in lamina I neurons, under the treatment conditions shown above. * $p < 0.05$ compared to control. All traces are presented as mean (darker line) \pm standard error (lighter shaded area). Scale bar x axes = 100 ms, y axes = 5 pA.

significantly less than that in control recordings without any NMDAR inhibitors (3.40 ± 0.18 pC; $n = 24$ neurons; $p = 0.047$; Fig. 3A,D). Subtracting average mEPSCs recorded in the presence of TCN-201 from the average control mEPSCs (Fig. 3B) yielded a TCN-201-sensitive current (charge transfer -0.54 ± 0.31 pC), which formed a portion of the initial part of the NMDAR component of the mEPSCs. In a subset of neurons we tested the effect of both 3 μ M and 10 μ M TCN-201 on NMDAR mEPSCs and found no difference in inhibition, indicating that a maximal TCN-201 inhibitory effect was reached in our spinal cord slice recordings (3 μ M TCN-201 inhibited mEPSCs by $17 \pm 3\%$, $n = 2$; 10 μ M TCN-201 inhibited mEPSCs by $20 \pm 2\%$, $n = 2$). In order to confirm the effect of TCN-201, we utilized another GluN2A antagonist, Zn^{2+} , at a concentration (200 nM free extracellular Zn^{2+}) reported to preferentially inhibit GluN2A-containing receptors over GluN2B-, C-, or D- containing receptors²⁰. We found that administering Zn^{2+} caused a reduction in NMDAR charge transfer of $16 \pm 5\%$ ($n = 6$, $p = 0.025$) (Supplementary Figure 2). The percentage reduction in mEPSC charge transfer by Zn^{2+} was not significantly different from that of TCN-201 ($p = 0.78$). The relatively small effect of TCN-201 and Zn^{2+} might have been attributable to a basal level of Zn^{2+} in the extracellular solution, sufficient to partially suppress GluN2A-mediated NMDAR currents. However, we found that administering the Zn^{2+} chelator, tricaine, had no effect on mEPSCs (Supplementary Figure 2), demonstrating that there was no ongoing Zn^{2+} -mediated masking of a GluN2A component of the mEPSCs. Together, these findings indicate that there is an early portion of the NMDAR component of mEPSCs in lamina I neurons mediated by GluN2A-containing receptors.

We tested for the involvement of GluN2B-containing NMDARs by treating slices with the GluN2B antagonist, Ro25-6981 (1 μ M). At this concentration Ro25-6981 inhibits GluN2B-containing NMDARs by more than 95% while not affecting GluN2A-, C-, or D-containing

NMDARs²². We found that administering Ro25-6981 caused a significant reduction in the NMDAR component of mEPSCs (Fig. 3A, D): the NMDAR charge transfer in the presence of Ro25-6981 was reduced to 1.23 ± 0.18 pC ($n = 12$ neurons; $p = 4.9 \times 10^{-9}$ compared with mEPSCs in control recordings without any NMDAR blockers). The average Ro25-6981-sensitive current (charge transfer -2.17 ± 0.25 pC), obtained by subtracting mEPSCs recorded in the presence versus in the absence of Ro25-6981 (Fig. 3B), was found to be more slowly decaying than the TCN-201-sensitive current. The reduction in the mEPSC amplitude by Ro25-6981 together with the more prolonged decay of the Ro25-6981-sensitive current indicates that a portion of the NMDAR component of mEPSCs is mediated by GluN2B-containing receptors. Surprisingly, the peak amplitude and the charge transfer of the Ro25-6981-sensitive current of mEPSCs were substantially larger than those of the TCN-201-sensitive current of mEPSCs in the lamina I neurons.

Moreover, we noted that the sum of the charge transfers of the TCN-201-sensitive and Ro25-6981-sensitive currents was less than that of the overall NMDAR component of the averaged mEPSCs. Therefore, we questioned whether the NMDAR component of the mEPSCs was fully accounted for by NMDARs containing GluN2A or GluN2B. We tested this by recording mEPSCs in the presence of both TCN-201 and Ro25-6981, and found a slowly decaying component of the mEPSCs that was resistant to these blockers (Fig. 3C, D). Such a component was not observed in recordings done in the presence APV (Fig. 3C), indicating that the TCN-201- and Ro25-6981-resistant component was mediated by NMDARs.

GluN2D NMDARs in mEPSCs of adult lamina I neurons. Because a substantial fraction of the mEPSCs was resistant to TCN-201 and Ro25-6981, we wondered whether receptors containing NMDAR subunits other than GluN2A or GluN2B may contribute to excitatory synaptic currents in adult lamina I neurons. In order to

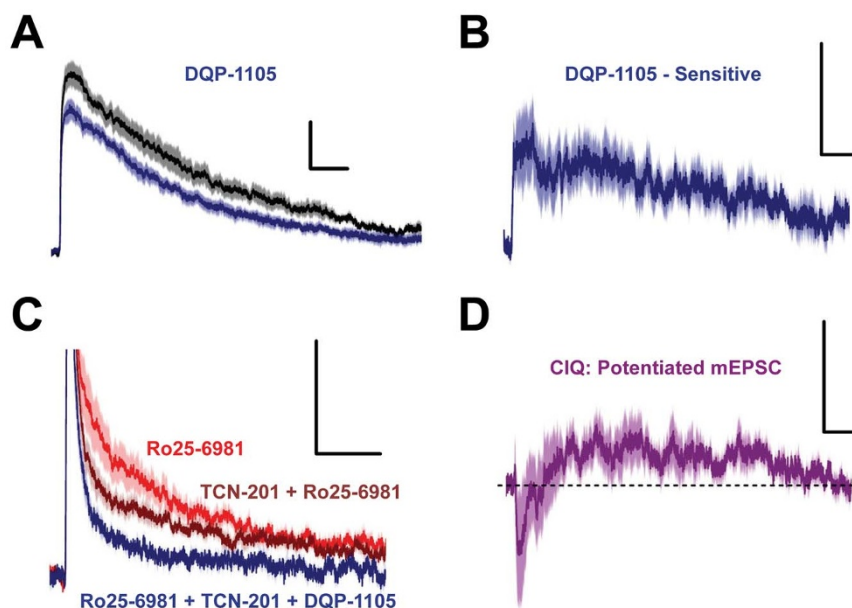


Figure 4 | NMDAR mEPSCs contain a slow decaying, DQP-1105-sensitive component in adult lamina I neurons. (A) Average mEPSC traces (with 1 s sampling duration) from lamina I neurons at +60 mV before and during perfusion of 10 μM DQP-1105 (blue, $n = 7$). (B) Plot of average DQP-sensitive mEPSC at +60 mV, based on control minus DQP-1105 treatment subtractions from data in (A) ($n = 7$). (C) Average mEPSC traces at +60 mV including neurons treated with 1 μM Ro25-6981 (red, $n = 12$), neurons treated with 3 μM TCN-201 and 1 μM Ro25-6981 (maroon, $n = 7$), and neurons treated with 3 μM TCN-201, 1 μM Ro25-6981, and 10 μM DQP-1105 (blue, $n = 5$). The mEPSC peak was truncated to highlight changes in the residual slow NMDAR component. (D) Plot of average CIQ-potentiated mEPSC based on subtraction of control mEPSCs from CIQ treatment mEPSCs ($n = 6$ neurons). Scale bar x axes = 100 ms, y axes = 5 pA.

test for non-GluN2A and non-GluN2B containing receptors we utilized DQP-1105, which inhibits GluN2C- and GluN2D-containing receptors with IC₅₀ values up to 50-fold lower than those for GluN2A- or GluN2B-containing receptors²³. We used DQP-1105 at a concentration (10 μM) at which currents from GluN2C- and GluN2D-containing currents are suppressed by about 65% and 85%, respectively, but at which there is only a minimal effect on GluN2A-containing and no effect on GluN2B-containing receptors²³. We found that administering DQP-1105 significantly reduced the NMDAR component of the mEPSCs (Fig. 4A–C). Average NMDAR charge transfer was reduced from 3.47 ± 0.22 pC before administering DQP-1105 to 2.61 ± 0.16 pC during DQP-1105 ($n = 8$ neurons; $p = 0.000046$), in the absence of any other NMDAR blockers (Fig. 4A,B). To specifically examine the TCN-201- and Ro25-6981-resistant component of NMDAR mEPSCs we compared mEPSCs in neurons treated with TCN-201- and Ro25-6981 with or without DQP-1105 (Fig. 4C). The TCN-201- and Ro25-6981-resistant component was significantly reduced by DQP-1105: charge transfer without DQP-1105 was 0.89 ± 0.11 pC ($n = 7$ neurons) whereas that in the presence of DQP-1105 was 0.33 ± 0.07 pC ($n = 5$ neurons; $p = 0.0034$). Moreover, the DQP-1105-sensitive current was much more prolonged than either the TCN-201- or Ro25-6981-sensitive currents (cf. Fig. 3B vs Fig. 4B, quantified below).

To independently test for a contribution of NMDAR subunits other than GluN2A or GluN2B we used the positive allosteric modulator, CIQ, which potentiates currents through NMDARs containing GluN2C or GluN2D²⁴. We found that administering CIQ (20 μM) had a dual effect on mEPSCs: CIQ inhibited an early portion of the mEPSCs but significantly increased a late portion of the NMDAR component of mEPSCs, beginning approximately 100 ms from mEPSC onset (Fig. 4D, $p < 0.05$). Moreover, the decay rate of NMDAR mEPSCs was significantly slowed by CIQ: the decay time constant without CIQ was 260 ± 30 ms ($n = 7$ neurons) whereas that in the presence of CIQ was 360 ± 40 ms ($n = 7$ neurons, $p = 0.037$). The inhibition of the early portion of the NMDAR component of the mEPSCs is attributable to weak inhibition of GluN2B-

containing NMDARs by CIQ at a concentration of 20 μM ²⁴. However, inhibition of GluN2B receptors cannot account for the potentiation of the late portion of the mEPSCs by CIQ. Thus, together with the resistance to TCN-201 and Ro25-6981, the blockade by DQP-1105 and the potentiation by CIQ demonstrate that the mEPSCs have a component mediated by NMDAR subunits other than GluN2A or GluN2B. The pharmacological profiles of DQP-1105 and CIQ may suggest GluN2C or GluN2D subunits. However, the component of the mEPSCs blocked by DQP-1105 and potentiated by CIQ was much more prolonged than can be accounted for by GluN2C-containing NMDARs²⁵. Moreover, expression of GluN2C mRNA and protein is negligible in the spinal dorsal horn^{26–29}. Therefore, we conclude that there is a component of excitatory synaptic currents in adult lamina I neurons mediated by GluN2D-containing NMDARs.

Differential contributions of GluN2A, GluN2B and GluN2D NMDARs in mEPSCs of adult lamina I neurons. Our findings above indicate that the NMDAR component of the lamina I mEPSCs is comprised of pharmacologically separable parts which may be mediated by contributions of GluN2A-containing, GluN2B-containing or GluN2D-containing NMDARs. Because the deactivation rates of NMDARs are highly dependent upon the GluN2 subunit composition of the receptor²⁵, we examined the decay rates of the portions of the mEPSCs that were inhibited by the pharmacological blockers. The decay time constants were calculated from mono-exponential fitting of the averaged blocker-sensitive currents: TCN-201-sensitive, 85 ms; Ro25-6981-sensitive, 281 ms; and DQP-1105-sensitive, 794 ms (Fig. 5A). These decay time constants are consistent with deactivation time constants of recombinant NMDARs containing GluN1 together with GluN2A, GluN2B or GluN2D, respectively^{3,25}.

Therefore, we calculated the relative proportion of the total NMDAR synaptic current sensitive to each of the blockers. We found that the TCN-201-, Ro25-6981- and DQP-1105-sensitive portions of the peak NMDAR component of the mEPSCs were $16 \pm 7\%$ ($n = 12$

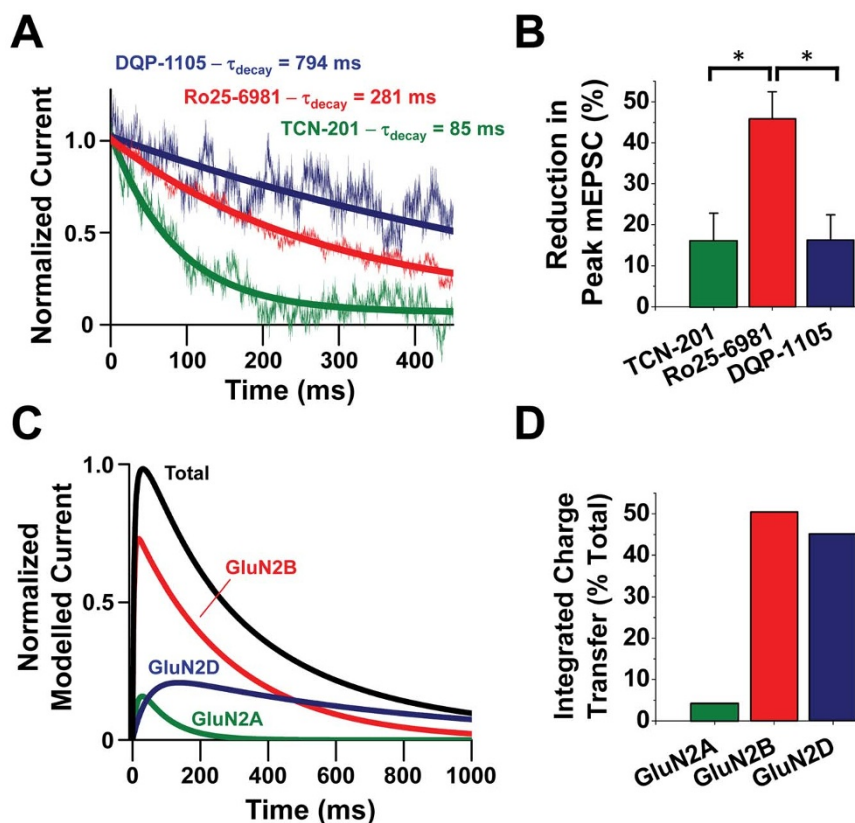


Figure 5 | Relative contributions of GluN2A, GluN2B and GluN2D to overall synaptic NMDAR currents in adult lamina I neurons. (A) Normalized mEPSC decay phases (lighter traces) for the DQP-1105-sensitive (blue, $n = 7$ neurons), Ro25-6981-sensitive (red, $n = 9$ neurons) and TCN-201-sensitive (green, $n = 7$ neurons) components of mEPSCs at $+60$ mV, derived from paired recordings before and during antagonist perfusion. Monoexponential fittings of DQP-1105- (blue), Ro25-6981- (red) and TCN-201- (green) sensitive mEPSCs are illustrated as darker lines, with associated decay time constants shown in the corresponding color. (B) Histogram quantifying the percent reduction in peak mEPSCs at $+60$ mV by treatment with $3 \mu\text{M}$ TCN-201 (green, $n = 12$), $1 \mu\text{M}$ Ro25-6981 (red, $n = 12$), or $10 \mu\text{M}$ DQP-1105 (blue, $n = 7$). * $p < 0.05$ (C) Modeled GluN2 subtype-mediated synaptic NMDAR currents in lamina I neurons using the difference of a decaying and rising exponential equation. The equation included decay time constants and relative amplitudes from panels (A) and (B), respectively, and rise time constants from published reports (see Methods). Calculated GluN2A, 2B, and 2D-mediated synaptic NMDAR currents are shown as green, red, and blue traces, respectively. The sum of the individual GluN2-subtype components is shown as a black trace. (D) Histogram of integrated charge transfer through GluN2 subtype-mediated synaptic NMDARs relative to total NMDAR charge transfer, calculated as the total area under the curve for the curves partially illustrated in (C).

cells), $46 \pm 7\%$ ($n = 8$ cells), and $16 \pm 6\%$ ($n = 7$ cells), respectively (Fig. 5B). From the proportionate peak values and decay time constants determined in the present experiments, together with published activation time constants for GluN2 subtypes^{3,30,31} we estimated the relative GluN2A-, GluN2B- and GluN2D-sensitive portions of the synaptic NMDAR currents (Fig. 5C). As the simplest approach, we summed the individual blocker-sensitive portions and found that the sum gave a total estimated NMDAR mEPSC (Fig. 5C), the time course of which was not significantly ($p = 0.22$) different from that of the NMDAR-mediated component of the mEPSCs measured experimentally (estimated $\tau_{\text{decay}} = 371$ ms, measured $\tau_{\text{decay}} = 320 \pm 40$ ms, $n = 14$ cells). Integrating the total charge transfer during the estimated mEPSCs revealed that GluN2B-containing NMDARs accounted for 50% of the total charge, similar to the proportionate contribution to the peak NMDAR current (Fig. 5D). In contrast, the TCN-201- and DQP-1105-sensitive portions each accounted for 16% of the peak NMDAR current, but the charge transfer mediated by estimated GluN2A-containing NMDARs was only 4% of the total whereas that carried by estimated GluN2D-containing NMDARs was 45% (Fig. 5D). Thus, we infer that the majority of overall synaptic NMDAR current in adult lamina I neurons may be mediated by GluN2B-containing NMDARs, with a substantial component mediated by GluN2D and only a small component mediated by GluN2A.

NMDAR components of unitary evoked EPSCs of adult lamina I neurons. As mEPSCs are generated from a number of different synapses^{19,32} the NMDAR-mediated component may derive from the three GluN2 subunits contributing in a fixed GluN2A : GluN2B : GluN2D ratio at each synapse. Alternatively, individual synapses may be heterogeneous, with distinctive GluN2A : GluN2B : GluN2D combinations at different synapses. In order to determine whether individual excitatory synapses of lamina I neurons are a homogenous or heterogeneous representation of the overall population of mEPSCs, we investigated unitary EPSCs (uEPSCs) evoked by stimulating a single synaptic connection to the neuron recorded. During recordings in the absence of TTX, we evoked uEPSCs by electrically stimulating in the dorsal root entry, which contains axons of primary afferent neurons that are monosynaptically connected to lamina I neurons. We found that by gradually increasing stimulation intensity we evoked all-or-none post-synaptic responses (Fig. 6Aa,b). The minimal stimulation-evoked responses had the following characteristics: a sharp stimulation threshold; a consistent latency, amplitude and failure rate; and blockade by TTX. Thus, we considered the minimal stimulation responses to be action potential-mediated uEPSCs. When the resting membrane potential was held at -60 mV the uEPSCs were rapidly decaying and blocked by CNQX (not illustrated). Holding the membrane potential at $+60$ mV revealed a slowly decaying component that

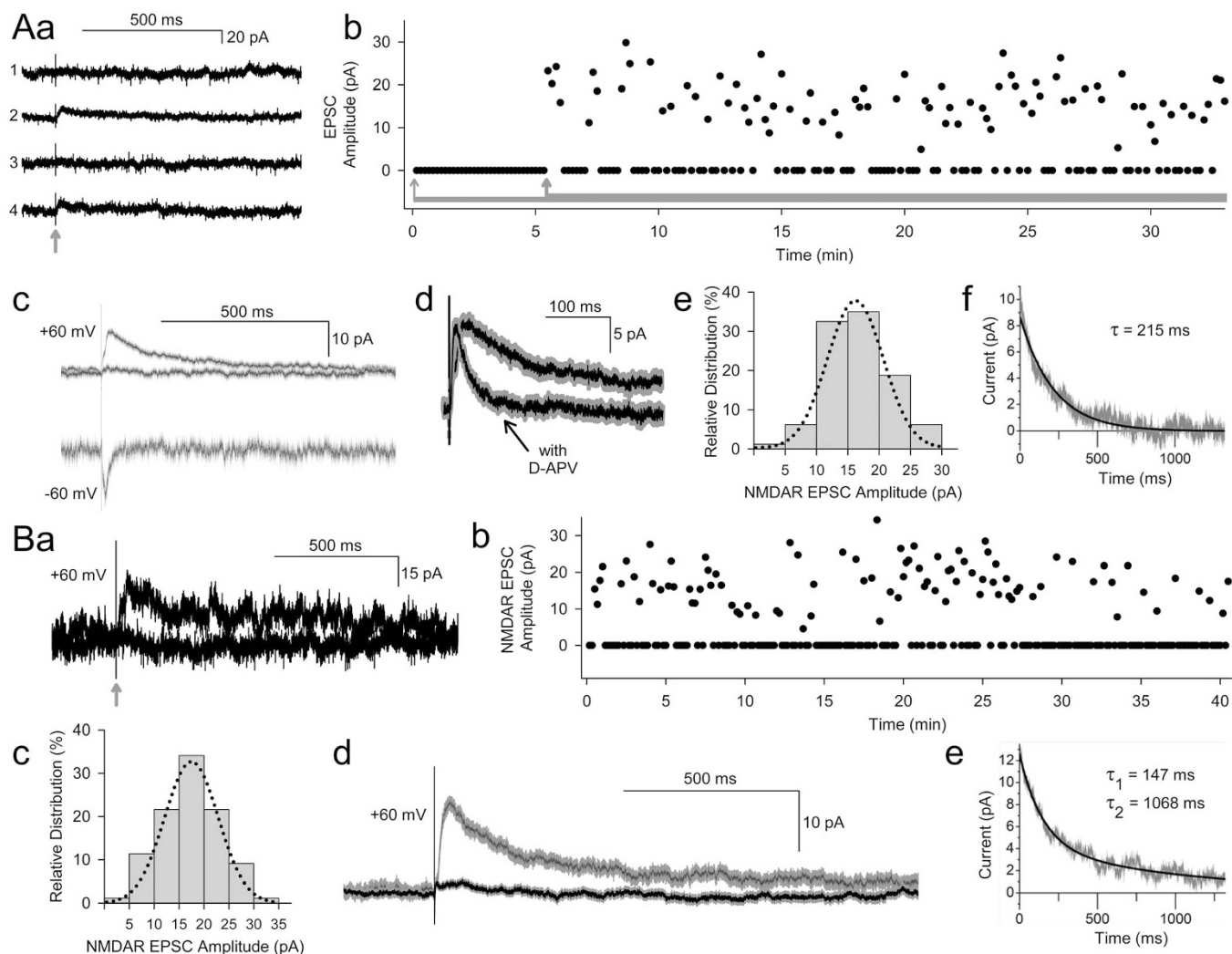


Figure 6 | NMDAR components of unitary-evoked EPSCs from adult rat lamina I neurons. (A) Recordings of unitary-evoked EPSCs from a representative adult rat lamina I neuron. (a) Sample traces showing individual consecutive all-or-none EPSCs at +60 mV elicited by minimal stimulation of a sensory afferent dorsal root. Traces 1 and 3 show synaptic failures while traces 2 and 4 show successful EPSCs in response to minimal sensory afferent stimulation (arrow indicates stimulus artifact). (b) Scatter plot of successful EPSC responses and synaptic failures over time (thick gray bar) evoked by minimal stimulation (0.2 Hz). Each point greater than 0 represents the EPSC amplitude of an individual successful event while each point at 0 indicates an individual failure event (~60% failure rate). Subthreshold sensory afferent stimulation, indicated by the thin gray bar, yielded a 100% failure rate. (c) Top: Averaged traces showing successful unitary EPSCs (+60 mV) and synaptic failures. Bottom: Averaged trace showing successful EPSCs recorded at -60 mV. (d) Averaged trace illustrating D-APV (100 μ M) blocked a slow decaying component of unitary EPSCs (+60 mV). (e) NMDAR amplitude histogram showing relative distribution for successful evoked EPSC responses, fit with a single Gaussian function. (f) Single exponential fitting (best fit) of the decay component of the average EPSC at +60 mV. (B) Recordings of unitary-evoked EPSCs from another adult lamina I neuron. (a) Sample individual traces at +60 mV demonstrating a successful EPSC and a failure in response to minimal stimulation of a sensory afferent dorsal root (the stimulus artifact is indicated by the arrow). (b) Scatter plot of successful NMDAR EPSC responses and failures (~50% failure rate) over time evoked by minimal stimulation (0.2 Hz). (c) NMDAR amplitude histogram showing relative distribution for successful evoked EPSC responses, fit with a single Gaussian function. (d) Averaged traces showing successful unitary EPSCs (+60 mV) and synaptic failures. (e) Double exponential fitting (best fit) of the decay component of the average unitary EPSC at +60 mV.

was blocked by D-APV (100 μ M; Fig. 6Ac,d). Thus, the uEPSCs had fast AMPAR- and slow NMDAR-mediated components.

We analyzed the NMDAR-mediated component recorded at +60 mV and found that the amplitudes of the minimal-stimulation evoked responses for each cell were normally distributed (e.g. Fig. 6Ae), consistent with the responses being generated at a single synapse. Because the different GluN2 subtypes in the mEPSCs were readily distinguished on the basis of differing decay time constants, as shown above, we investigated the potential contributions of different GluN2s to the unitary synaptic responses by examining the decay time constants of the uEPSCs. We found that the decay time constants of the NMDAR component of the uEPSCs were consistent

throughout each single-synapse recording period. In contrast, there was large variability in the NMDAR decay time constants between single-synapse recordings. For example, the NMDAR component of the uEPSC in Figure 6A was best fit with a single exponential, $\tau = 215$ ms. On the other hand, the decay of the NMDAR component at a synapse on a different lamina I neuron, shown in Figure 6B, was best fit as a sum of two exponentials with $\tau_1 = 147$ ms and $\tau_2 = 1068$ ms. The large between-recording variability in the decay time constants of the NMDAR components is not consistent with a homogenous distribution of GluN2 subunits at all primary afferent lamina I neuron synapses. Rather, the between-recording time constant differences imply that GluN2 subunit composition varies synapse-by-synapse.



The majority of individual primary afferent-lamina I neuron synapses ($n = 5$ of 8; e.g. Fig. 6Af) had an NMDAR component with a decay time constant between 200 and 400 ms, consistent with GluN2B-containing receptors. At a subset of synapses ($n = 3$ of 8) the decay time constant of an NMDAR component was less than 80 ms, suggestive of GluN2A-containing receptors. Moreover, uEPSCs were reduced by administering Zn^{2+} (200 nM free concentration) in only one of three synapses tested (Supplementary Figure 3); Zn^{2+} had no effect on the uEPSCs in the other two synapses. That only a subset of primary afferent-lamina I neuron synapses had a component with characteristics consistent with GluN2A-containing NMDARs could not be attributed to extracellular Zn^{2+} contamination because the Zn^{2+} chelator, tricine, caused the NMDAR charge transfer to remain at $99.4\% \pm 7.8\%$ ($n = 6$) of that before tricine (Supplementary Figure 3). Strikingly, we found a subpopulation of primary afferent-lamina I neuron synapses ($n = 3$ of 8; e.g. Fig. 6Be) with a component having a long decay time constant, ranging from 1068 ms to 3152 ms. In one of the latter recordings, with a decay time constant of 1638 ms, we applied DQP (10 μ M) which reduced the charge transfer from 6.11 to 4.34 pC, suggesting a synaptically-evoked response mediated by GluN2D-containing NMDARs.

Discussion

We describe here spontaneously-occurring miniature EPSCs and action potential-evoked unitary EPSCs in lamina I neurons in the adult spinal cord that are characterized by a fast AMPAR-mediated component and slower NMDAR-mediated components. Hence, glutamatergic synapses in adult lamina I neurons show fundamental characteristics typical of fully developed, glutamatergic synapses in the adult CNS. However, we find that the NMDAR-mediated components of the mEPSCs and uEPSCs are dominated by GluN2B and GluN2D-containing receptors, demonstrating that excitatory synapses on lamina I neurons are highly distinct from glutamatergic synapses described elsewhere in the adult CNS. The mEPSCs were recorded in the presence of TTX to block action potential-dependent transmitter release and of the calcium channel blocker Cd^{2+} to prevent the possibility that the mEPSCs were evoked secondary to calcium entry through voltage-gated calcium channels. The uEPSCs were all-or-none and showed a clear unimodal, normal distribution. Thus, we conclude that the mEPSCs and uEPSCs we recorded are due to release of individual quanta and are, therefore, mediated by activation of synaptic, as opposed to extrasynaptic, NMDARs.

One major distinguishing feature of the synaptic NMDAR responses in adult lamina I neurons was the small relative proportion mediated by GluN2A-containing NMDARs, accounting for approximately 16% of the peak current and less than 5% of total synaptic charge transfer. The small proportionate size of the GluN2A-mediated component in lamina I neurons contrasts with that in, for example, the adult hippocampus and cortex, where the GluN2A-mediated component accounts for the majority of NMDAR synaptic responses^{4–8}. The GluN2A-mediated component might have been reduced at lamina I synapses if there was a substantial level of extracellular Zn^{2+} during our recordings, as GluN2A-containing NMDARs are differentially inhibited by Zn^{2+} at nanomolar concentrations²⁰. However, we observed that the NMDAR component of both the mEPSCs and the uEPSCs was unaffected by chelating Zn^{2+} with tricine. Thus, there was no Zn^{2+} blockade to account for the proportionately low size of the GluN2A component of synaptic NMDAR responses. It has been shown immunohistochemically that GluN2A protein levels are low at synapses within the superficial dorsal horn of adult rats³³. Hence, the simplest explanation for the proportionately low size of the GluN2A component of mEPSCs and uEPSCs is that there is low expression of GluN2A-containing receptors at glutamatergic synapses of lamina I neurons in the adult spinal cord.

In contrast to the small contribution of GluN2A at adult lamina I synapses, approximately half of the peak synaptic NMDAR current and charge transfer was mediated by GluN2B-containing NMDARs. This conclusion follows from the reduction in the NMDAR component of mEPSCs caused by Ro25-6981, which we used at a concentration known to inhibit GluN2B-containing receptors without affecting GluN2A, 2C, or 2D NMDARs²². GluN2B-containing receptors may be comprised of GluN1 together with only GluN2B (GluN1/2B/2B) or with GluN2A as well as GluN2B (GluN1/2A/2B). Both GluN1/2B/2B and GluN1/2A/2B receptors are inhibited by benzylpiperidines, such as ifenprodil and derivatives like Ro25-6981^{34,35}. However, such GluN2B inhibitors maximally suppress GluN1/2A/2B receptors by only about 20%, leaving a residual GluN1/2A/2B-mediated current with enhanced sensitivity to GluN2A blockers³⁴. Thus, if the reduction in the NMDAR component of the mEPSCs by Ro25-6981 had been due to blockade of GluN1/2A/2B receptors, then about 80% of the current would have remained. In this scenario, TCN-201 would have blocked the putative residual GluN1/2A/2B current³⁴ and therefore, TCN-201 would have had a much larger effect in the presence than in the absence of Ro25-6981. However, we observed that the magnitude of the effect of TCN-201 with Ro25-6981 was similar to that without Ro25-6981, arguing against a dominant contribution of GluN1/2A/2B receptors to the NMDAR component of the mEPSCs. Moreover, the decay time constant of the Ro25-6981-sensitive component of the mEPSCs was 281 ms, which is close to that reported for the GluN1/2B/2B component of synaptic currents at other central synapses (e.g. 315 ms reported by Westbrook and colleagues³⁶) and is far from that of GluN1/2A/2B currents (e.g. 79 ms in³⁶). Thus, with the current understanding of the pharmacological characteristics of tri-heteromeric NMDARs, our findings suggest that the GluN2B component of the synaptic NMDAR responses in lamina I neurons is mediated by GluN1/2B/2B receptors, although we cannot eliminate the possibility of a contribution by GluN1/2A/2B.

Strikingly, we found that NMDAR-mediated synaptic responses in adult lamina I neurons decay much more slowly than can be accounted for by only GluN2A- and GluN2B-containing NMDARs. The very slow component of the mEPSCs was resistant to TCN-201 and Ro25-6981, but was inhibited by DQP-1105 and was potentiated by CIQ. DQP-1105 and CIQ may act on GluN2C- and on GluN2D-containing NMDARs^{23,24}. However, the deactivation time constant for GluN2C-containing NMDARs is approximately 300 ms^{3,25} whereas the mEPSCs and the uEPSCs decayed much more slowly. GluN2D NMDARs have decay time constants between 600 ms and 3500 ms, depending on the specific GluN1 isoform co-expressed³⁷, which matches the range of the decay time constants we observed. Thus, the decay time constants of the very slow component of the NMDAR synaptic responses we found are inconsistent with GluN2C receptors but are consistent with GluN2D NMDARs. In addition, GluN2D mRNA and protein are expressed in the superficial dorsal horn³⁸ whereas GluN2C is not detected^{27–29}. DQP-1105 may inhibit GluN2A-containing NMDARs in addition to GluN2D-containing receptors, although the potency at GluN2A-containing receptors is reported to be 4- to 50-fold less than that at GluN2D-containing receptors²³. The possibility of inhibiting GluN2A- as well as GluN2D-containing NMDARs would have been problematic if we had only tested DQP-1105 on its own. However, we also tested the effects of DQP-1105 in the presence of TCN-201 and Ro25-6981. Under these recording conditions, the TCN-201-resistant/Ro25-6981-resistant component of the mEPSC was inhibited by DQP-1105. Taking together our present findings and those in the literature, the most parsimonious interpretation is that GluN2D-containing receptors mediate the most slowly-decaying component of synaptic NMDAR responses in adult lamina I neurons. Future studies to investigate this possibility further could include molecular loss-of-function approaches



to complement the pharmacological and biophysical approaches used here.

There is evidence that NMDARs containing the GluN2D subtype may contribute to agonist-evoked or synaptically-activated NMDAR currents in neurons from several brain regions^{24,39,40}. In studies from the hippocampus and cerebellum, genetic, biophysical, and pharmacological experiments support a preferential contribution of GluN2D-containing receptors to somatic, agonist-evoked responses over synaptically-evoked NMDAR responses^{41–44}. Synaptic NMDAR responses with very slow decay have been observed in striatal neurons⁴⁵, although pharmacological inhibitors of GluN2D-containing receptors were not tested. In studies from substantia nigra and hippocampal neurons, blockers of GluN2D including UBP-141, UBP-145 and PPDA have been reported to inhibit synaptic NMDAR responses^{46–48}. A possible explanation put forward for the molecular basis of such synaptic responses has been that these synaptic NMDAR currents may be mediated by triheteromeric NMDARs composed of GluN1, GluN2B, and GluN2D subunits^{46,48}. This interpretation is consistent with reports of native triheteromeric GluN1/2B/2D receptors in rat brain^{39,41,49,50}.

It is possible that like in the brain, GluN1/2B/2D receptors could potentially contribute to synaptic NMDAR responses in lamina I neurons. However, we found that the DQP-1105-sensitive NMDAR component of the mEPSCs in lamina I neurons is more prolonged than is the Ro25-6981-sensitive component. At synapses in the brain where GluN2D-blocker sensitive currents are attributed to putative GluN1/2B/2D receptors, the decay rates are similar to the GluN2B-blocker sensitive currents^{46,48}. Moreover, the decay rates of DQP-1105-sensitive synaptic currents in lamina I neurons were comparable to GluN1/2D/2D diheteromeric receptors^{25,37}. Hence, although we cannot exclude a potential contribution from triheteromeric GluN1/2B/2D receptors, it appears more likely that the majority of GluN2D-containing receptors at lamina I synapses are GluN1/2D/2D diheteromeric NMDARs.

That neurons in lamina I may have synaptic NMDAR responses mediated by GluN2D-containing receptors is consistent with evidence that such receptors may be functionally expressed in neurons in the superficial dorsal horn. For example, MacDermott and colleagues identified a component of the current responses evoked by exogenously administered NMDA in subsets of lamina I neurons and lamina II neurons with a low sensitivity to blockade by extracellular Mg^{2+} , indicative of GluN2C/D-containing receptors^{51,52}. In somatic patch recordings on adult lamina II spinal cord neurons, Momiyama and colleagues demonstrated that a low conductance NMDAR component has single channel properties consistent with GluN2D-containing NMDARs^{40,53,54}. Based on comparisons between these single-channel NMDAR currents and evoked synaptic NMDAR currents in lamina II neurons, it has been proposed that GluN2B and GluN2D-containing NMDARs are localized to extrasynaptic sites in dorsal horn neurons^{9,53}. Our findings do not exclude extrasynaptic GluN2D-containing receptors in addition to the synaptically-activated ones we have identified here.

The inhibitory effects of the subtype-selective pharmacological blockers on the peak of the NMDAR mEPSCs were relatively consistent between neurons. Thus as a first pass approximation, we estimated the relative proportion of GluN2A : GluN2B : GluN2D-containing NMDARs at lamina I synapses, and found a consistent, dominant contribution by putative GluN2B-containing receptors. By contrast to the mEPSCs, the kinetics of the NMDAR-component of the uEPSCs varied greatly from synapse to synapse suggesting large variability in the relative contributions of GluN2A, 2B, and 2D subunits at individual synapses. There are two main implications of this high degree of synapse-to-synapse variability. First, lamina I neurons have a mechanism, or mechanisms, to differentially traffic, target or stabilize NMDARs of specific subunit compositions to distinct synapses. Second, in as much as the proportion of GluN2A :

GluN2B may be critical for determining the sign and magnitude of activity-dependent synaptic plasticity^{55,56}, then different synapses of a given lamina I neuron may undergo distinct forms of synaptic plasticity. The differences in synaptic plasticity may occur even if the synapses receive the same frequency and pattern of input. Moreover, from the discovery of synapses with GluN2D-containing receptors it is conceivable that these receptors contribute to synaptic plasticity.

An important functional consequence of the large proportionate contribution of GluN2B- and GluN2D-containing NMDARs and of their slow deactivation kinetics is that adult lamina I glutamatergic synapses will have a much higher propensity to undergo temporal summation than will canonical GluN2A-dominated synapses. NMDAR-mediated temporal summation, often referred to as 'windup', is a hallmark and crucial characteristic of the pain integration and transmission network in the dorsal horn^{14,57}. Lamina I neurons are prominent within this pain network and spinal lamina I forms a distinct output pathway from this spinal network to the pain networks in the brain. The large proportionate contribution of GluN2B-containing, and particularly of GluN2D-containing, synaptic NMDAR currents provides the molecular underpinning for the slow, prolonged and feedforward excitation that is a fundamental property of pain.

Methods

Animals. All animal experiments were performed in accordance with the animal care regulations and policies of the Canadian Council on Animal Care, with detailed experimental procedures approved by the Animal Care Committee at the Hospital for Sick Children, Toronto. We used male adult (350 g to 450 g) Sprague Dawley rats for all experiments except for the initial mEPSC characterization studies (Fig. 2), where we also used P21 to P25 Sprague Dawley rats.

Spinal cord isolation. We anaesthetized male adult Sprague Dawley rats through intraperitoneal injection of 20% (wt/vol) urethane (Sigma). As previously described⁵⁸, we rapidly dissected out the lumbar spinal cord through ventral laminectomy and immediately placed the cord in an ice-cold protective modified artificial cerebrospinal fluid (aCSF) solution containing (in mM): 50 sucrose, 92 NaCl, 15 D-Glucose, 26 $NaHCO_3$, 5 KCl, 1.25 NaH_2PO_4 , 0.5 $CaCl_2$, 7 $MgSO_4$, 1 kynurenic acid, and bubbled with 5% $CO_2/95\% O_2$. We removed all meninges and ventral roots from the lumbar cord under a dissecting microscope, with additional dorsal root removal for mEPSC recording experiments (Figs. 1 to 5). Parasagittal spinal cord slices were used for all mEPSC experiments: we glued a lumbar spinal cord section (L3–L6) to the vibratome tray in a parasagittal orientation and thin slices (300 μm) were cut with a blade advance speed of 0.01 mm/s and amplitude of 3 mm. For minimal stimulation uEPSC recording experiments (Fig. 6), we cut 500 μm thick transverse lumbar spinal cord slices containing dorsal rootlets. Following sectioning, spinal cord slices were allowed to recover for 50 minutes at 34°C in a pACSF solution that lacked kynurenic acid. We then removed the slice recovery chamber from the heated water bath and allowed it to passively cool down to room temperature (20 to 22°C).

Electrophysiological recordings on lamina I spinal cord neurons. We visualized spinal cord slices using the IR-DIC optics of a Zeiss Axioskop 2 FS plus microscope (Gottingen, Germany). Recordings of lamina I neurons were made from neuronal cell bodies located in the darker, striated region dorsal to the translucent tissue band (substantia gelatinosa) that demarcates lamina II⁹. The cellular location was confirmed by immunohistochemistry in a subset of recordings in which the cells were loaded with 0.1% lucifer yellow via the patch pipette. Lamina I was identified as the dorsal horn region within approximately 50 μm of the superficial white matter, containing lower neuronal density and the superficial region of CGRP labeling^{60,61}. We used two photon imaging to confirm that the recorded neurons had morphological characteristics of lamina I neurons^{62,63}, which are distinct from those of lamina II neurons (Fig. 1, Fig. S1). Moreover, the mEPSCs in lamina I neurons were clearly distinct from those of neurons in lamina II, which were characterized by much smaller AMPAR and NMDAR components (Fig. S1). Thus, the recordings were made from bona fide lamina I neurons.

We pulled patch-clamp recording pipettes with typical resistances of 5 to 8 M Ω using borosilicate glass (BF150-86-10; Sutter Instruments, Navato, CA, USA) and a Sutter P97 puller and fire-polished the pipettes using a Narishige MF-830 microforge (Tokyo, Japan). The external recording solution consisted of an artificial cerebrospinal fluid (aCSF) solution containing (in mM): 125 NaCl, 20 D-Glucose, 26 $NaHCO_3$, 3 KCl, 1.25 NaH_2PO_4 , 2 $CaCl_2$, and 1 $MgCl_2$ as well as 500 nM TTX, 10 $\mu M Cd^{2+}$, 10 μM strychnine and 10 μM bicuculline to block voltage-gated sodium channels, voltage-gated calcium channels, inhibitory glycinergic receptors and inhibitory GABAergic receptors, respectively. For a subset of experiments examining NMDAR-mEPSCs (as indicated in the Results section), we used aCSF solution that lacked addition of 1 mM $MgCl_2$. The internal patch pipette solution contained (in mM): 105



Cs-Gluconate, 17.5 CsCl, 10 BAPTA, 10 HEPES, 5 QX-314, 2 MgATP, and 0.5 Na₂GTP (pH = 7.25, 295 mOsm).

Patch-clamp recordings utilized a Multiclamp 700 B amplifier (Molecular Devices, Sunnyvale, CA, USA) connected to a personal computer running pClamp10 software through a Digidata 1440 A Data Acquisition System (Molecular Devices). Neurons typically had access resistances below 20 MΩ and leakage currents > -100 pA at a holding potential of -70 mV. Voltage-clamp recordings were digitized at 10 KHz and low-pass filtered at 2.4 kHz. Recordings were performed at room temperature for mEPSC recordings and at 28°C for uEPSC recordings. We used Clampfit10 to automatically detect mEPSCs, with Threshold Search Event Detection criteria of amplitude > 9 to 10 pA. We manually aligned all detected mEPSCs from their rising slope and also used this visual inspection to reject individual mEPSCs that did not display exponential decay kinetics or that had multiple mEPSC events during the sampling sweep. The duration of the sampling sweep was 500 ms, except for experiments in Figure 4A,B,D, where the sweep duration was 1000 ms to more accurately assess the decay of the DQP-sensitive component of the NMDARs. We generated averaged mEPSCs for time intervals ranging between 5 and 10 minutes, typically with 30 to 50 sweeps per averaged trace. The magnitude of the NMDAR mEPSC component at +60 mV was quantified through integration to determine NMDAR-mediated charge transfer. As the AMPAR mEPSC component decayed by greater than 95% by 40 ms at +60 mV (Fig. 2E), we integrated the area under the +60 mV mEPSCs from 40 ms to 500 ms to generate NMDAR charge transfer values. We generated averaged mEPSCs across multiple neurons for a given condition (i.e. -TCN-201 treatment), and plotted these averages as mean ± standard error of the mean (SEM), where the SEM bars are represented by a lighter shade.

For minimal stimulation experiments, only uEPSCs exhibiting a consistent latency and amplitude with each stimulus as well as a clear stimulation threshold (all-or-none post-synaptic response by gradually increasing stimulation intensity) and consistent failure rate were considered true minimal stimulation-evoked post-synaptic responses. uEPSCs were evoked using a bipolar tungsten electrode placed in the dorsal rootlet outside the spinal dorsal horn. Single stimuli were delivered at 0.2 Hz using an S48 Grass Stimulator.

Pharmacology. For electrophysiology experiments, D-AP5, bicuculline methochloride, (3-chlorophenyl) [3,4-dihydro-6,7-dimethoxy-1-[(4-methoxyphenoxy)methyl]-2(1H)-isoquinolinyl]methanone (CIQ), 4-(5-(4-bromophenyl)-3-(6-methyl-2-oxo-4-phenyl-1,2-dihydroquinolin-3-yl)-4,5-dihydro-1H-pyrazol-1-yl)-4-oxobutanoic acid (DQP-1105), (αR,βS)-α-(4-Hydroxyphenyl)-β-methyl-4-(phenylmethyl)-1-piperidinepropanol maleate (Ro25-6981), and (3-chloro-4-fluoro-N-[(4-[(2-phenylcarbonyl)hydrazino]carbonyl)phenyl]methyl]benzene-sulfonamide) (TCN-201) were obtained from Tocris Bioscience. TTX was obtained from Alomone labs. Unless otherwise indicated, all other compounds were obtained from Sigma-Aldrich. Pharmacology experiments were performed by either incubating slices in compound before and during recording, with unpaired comparisons to recordings from control-treated cells, or by acutely perfusing compound during recording, with paired comparisons to initial control recordings. For acute perfusion experiments, added compounds were allowed to perfuse into the recording chamber for 10 to 20 minutes to allow for sufficient diffusion and equilibration before the effects on mEPSCs were quantified. No significant differences were found between the two approaches, except for with Ro25-6981, where a greater inhibition of NMDAR charge transfer was produced by Ro25-6981 pretreatment (65% ± 5%, n = 12) compared to acute Ro25-6981 perfusion (48% ± 5%, n = 9). The reduced effect with acute Ro25-6981 perfusion could be caused by slow slice penetration and off-target absorbance by the hydrophobic Ro25-6981⁶⁴ and/or the activity-dependence of Ro25-6981 blockade²². Thus, the pretreatment approach was used exclusively for determining the magnitude of effect of Ro25-6981 on NMDAR mEPSCs.

To test for the contribution of GluN2A-containing NMDARs at lamina I synapses, we used TCN-201, an allosteric NMDAR inhibitor with selectivity against GluN2A-containing receptors. The binding of TCN-201 to a dimer interface between GluN1 and GluN2 inhibits NMDAR activity by reducing glycine potency^{21,65}. Agonists of the NMDAR glycine-binding site, glycine and serine, are tightly regulated in a sub-saturating concentration range at CNS synapses, including in the spinal cord^{4,66-68}. The concentration of TCN-201 (3 μM) we selected inhibits > 90% of GluN2A receptors in this high nanomolar glycine concentration range. Even if glycine reaches the low micromolar concentrations reported in the cerebrospinal fluid⁶⁵, 3 μM TCN-201 will inhibit approximately 80% of GluN2A receptors²¹. In positive control experiments, we tested TCN-201 on NMDAR EPSCs at hippocampal Schaffer collateral-CA1 synapses. We found that 3 μM TCN-201 inhibited NMDAR EPSCs by 50 ± 4% (n = 2) at these hippocampal synapses.

Two photon imaging. In a subset of experiments, we labeled neurons in spinal cord slices by including 0.1% lucifer yellow in the internal patch pipette solution during patch-clamp recordings. Immediately following recording, the slices were fixed in 4% PFA-containing phosphate-buffered solution (PBS) and stored at 4°C. We imaged slices in 0.1 M PBS under a Zeiss LSM710 Multiphoton Laser Microscope containing a NDD-GASP detector and a two-photon excitation chameleon laser (Coherent Inc., USA) tuned to 920 nm wavelength. Two-photon image stacks were obtained using a 20× water-immersion objective lens (Carl Zeiss Microscopy, Germany) and the Zen 2009 acquisition program (Carl Zeiss Microscopy, Germany). Image stacks were deconvolved, and flattened for publication using Volocity 6 3D image analysis software (Perkin Elmer, USA).

Slice immunohistochemistry. We washed slices in 0.1 M PBS under agitation to remove PFA, followed by blocking with 10% donkey serum/0.3% triton in 0.1 M PBS for one hour on agitation at room temperature. The primary antibodies rabbit anti-CGRP and mouse anti-NeuN were added at a 1 : 2000 dilution ratio in 3% donkey serum/0.3% triton in 0.1 M PBS. We incubated primary antibody-treated slices overnight on agitation at room temperature, followed by washing in 3% donkey serum/0.3% triton in 0.1 M PBS on agitation. We then agitated the slices for 3 hours at room temperature with secondary antibodies, Cy-5 donkey anti-mouse and Cy-3 donkey anti-rabbit, at a 1 : 1000 dilution ratio in 3% donkey serum/0.3% triton in 0.1 M PBS. The excess secondary antibody was washed off with 3% donkey serum/0.3% triton in 0.1 M PBS, and slices were mounted using fluoromount.

We imaged antibody-treated slices using a Zeiss AxioVert 200 Inverted Fluorescence microscope and Volocity 5 Acquisition software (Perkin Elmer, USA). Image stacks were taken at 5× and 20× objective magnifications. Deconvolution of images and the addition of scale bars were performed using Volocity 6 3D image analysis software. The two-photon images of neurons were brought down to scale with slice images, and the green channel containing the neuron was isolated using Photoshop CS5 (Adobe Systems Inc., USA). The green channel was then superimposed over the epifluorescent green signal for the neuron, and the epifluorescent green signal was removed.

Data analysis and curve fitting. We calculated decay time constants by least-squares fitting with one, two or three exponentials. Best-fit was determined by comparing R² for the respective fits. Relative GluN2 subtype-mediated synaptic NMDAR currents in lamina I neurons (Fig. 5C) were modeled using the difference of a decaying and rising exponential equation: $I(t) = A * ((e^{-t/\tau_{decay}}) - (e^{-t/\tau_{rise}}))$. A was the fractional blockade of the peak (Fig. 5B), τ_{decay} was the decay time constant of the blocker-sensitive difference currents calculated here (Fig. 5A), and τ_{rise} was the activation time constant for each of the GluN2 subtypes taken from published reports^{30,31}.

All data are given as means ± SEM. We performed statistical comparisons of data using the following, chosen as appropriate for each comparison: Student's paired or unpaired *t*-test, or one-way ANOVA followed by a Tukey's test for means comparison. We considered *p* < 0.05 to be statistically significant.

1. Traynelis, S. F. *et al.* Glutamate receptor ion channels: structure, regulation, and function. *Pharmacol Rev* **62**, 405–496 (2010).
2. Kalia, L. V., Kalia, S. K. & Salter, M. W. NMDA receptors in clinical neurology: excitatory times ahead. *Lancet Neurol* **7**, 742–755 (2008).
3. Paoletti, P., Bellone, C. & Zhou, Q. NMDA receptor subunit diversity: impact on receptor properties, synaptic plasticity and disease. *Nat Rev Neurosci* **14**, 383–400 (2013).
4. Papouin, T. *et al.* Synaptic and extrasynaptic NMDA receptors are gated by different endogenous coagonists. *Cell* **150**, 633–646 (2012).
5. Rodenas-Ruano, A., Chavez, A. E., Cossio, M. J., Castillo, P. E. & Zukin, R. S. REST-dependent epigenetic remodeling promotes the developmental switch in synaptic NMDA receptors. *Nat Neurosci* **15**, 1382–1390 (2012).
6. Quinlan, E. M., Olstein, D. H. & Bear, M. F. Bidirectional, experience-dependent regulation of N-methyl-D-aspartate receptor subunit composition in the rat visual cortex during postnatal development. *Proc Natl Acad Sci U S A* **96**, 12876–12880 (1999).
7. Matta, J. A., Ashby, M. C., Sanz-Clemente, A., Roche, K. W. & Isaac, J. T. mGluR5 and NMDA receptors drive the experience- and activity-dependent NMDA receptor NR2B to NR2A subunit switch. *Neuron* **70**, 339–351 (2011).
8. Ng, D. *et al.* Netol1 is a novel CUB-domain NMDA receptor-interacting protein required for synaptic plasticity and learning. *PLoS Biol* **7**, e41 (2009).
9. Cull-Candy, S. G. & Leszkiewicz, D. N. Role of distinct NMDA receptor subtypes at central synapses. *Sci STKE* **2004**, re16 (2004).
10. Monyer, H., Burnashev, N., Laurie, D. J., Sakmann, B. & Seeburg, P. H. Developmental and regional expression in the rat brain and functional properties of four NMDA receptors. *Neuron* **12**, 529–540 (1994).
11. Sheng, M., Cummings, J., Roldan, L. A., Jan, Y. N. & Jan, L. Y. Changing subunit composition of heteromeric NMDA receptors during development of rat cortex. *Nature* **368**, 144–147 (1994).
12. Wenzel, A., Fritschy, J. M., Mohler, H. & Benke, D. NMDA receptor heterogeneity during postnatal development of the rat brain: differential expression of the NR2A, NR2B, and NR2C subunit proteins. *J Neurochem* **68**, 469–478 (1997).
13. von Hehn, C. A., Baron, R. & Woolf, C. J. Deconstructing the neuropathic pain phenotype to reveal neural mechanisms. *Neuron* **73**, 638–652 (2012).
14. Woolf, C. J. & Salter, M. W. Neuronal plasticity: increasing the gain in pain. *Science* **288**, 1765–1769 (2000).
15. D'Mello, R. & Dickenson, A. H. Spinal cord mechanisms of pain. *Br J Anaesth* **101**, 8–16 (2008).
16. Todd, A. J. Neuronal circuitry for pain processing in the dorsal horn. *Nat Rev Neurosci* **11**, 823–836 (2010).
17. Woolf, C. J. & Salter, M. W. In *Melzack and Wall's Textbook of Pain* (eds McMahon, S. B. & Koltzenberg, M.) 91–106 (Elsevier, 2005).
18. Manabe, T., Renner, P. & Nicoll, R. A. Postsynaptic contribution to long-term potentiation revealed by the analysis of miniature synaptic currents. *Nature* **355**, 50–55 (1992).



19. Raastad, M., Storm, J. F. & Andersen, P. Putative Single Quantum and Single Fibre Excitatory Postsynaptic Currents Show Similar Amplitude Range and Variability in Rat Hippocampal Slices. *Eur J Neurosci* **4**, 113–117 (1992).
20. Paoletti, P., Ascher, P. & Neyton, J. High-affinity zinc inhibition of NMDA NR1-NR2A receptors. *J Neurosci* **17**, 5711–5725 (1997).
21. Hansen, K. B., Ogden, K. K. & Traynelis, S. F. Subunit-selective allosteric inhibition of glycine binding to NMDA receptors. *J Neurosci* **32**, 6197–6208 (2012).
22. Fischer, G. *et al.* Ro 25-6981, a highly potent and selective blocker of N-methyl-D-aspartate receptors containing the NR2B subunit. Characterization in vitro. *J Pharmacol Exp Ther* **283**, 1285–1292 (1997).
23. Acker, T. M. *et al.* Mechanism for noncompetitive inhibition by novel GluN2C/D N-methyl-D-aspartate receptor subunit-selective modulators. *Mol Pharmacol* **80**, 782–795 (2011).
24. Mullasseril, P. *et al.* A subunit-selective potentiator of NR2C- and NR2D-containing NMDA receptors. *Nat Commun* **1**, 90 (2010).
25. Vicini, S. *et al.* Functional and pharmacological differences between recombinant N-methyl-D-aspartate receptors. *J Neurophysiol* **79**, 555–566 (1998).
26. Karlsson, U. *et al.* Glutamate-induced currents reveal three functionally distinct NMDA receptor populations in rat dorsal horn - effects of peripheral nerve lesion and inflammation. *Neuroscience* **112**, 861–868 (2002).
27. Shibata, T., Watanabe, M., Ichikawa, R., Inoue, Y. & Koyanagi, T. Different expressions of alpha-amino-3-hydroxy-5-methyl-4-isoxazole propionic acid and N-methyl-D-aspartate receptor subunit mRNAs between visceromotor and somatomotor neurons of the rat lumbosacral spinal cord. *J Comp Neurol* **404**, 172–182 (1999).
28. Watanabe, M., Mishina, M. & Inoue, Y. Distinct spatiotemporal distributions of the N-methyl-D-aspartate receptor channel subunit mRNAs in the mouse cervical cord. *J Comp Neurol* **345**, 314–319 (1994).
29. Yung, K. K. Localization of glutamate receptors in dorsal horn of rat spinal cord. *Neuroreport* **9**, 1639–1644 (1998).
30. Banke, T. G., Dravid, S. M. & Traynelis, S. F. Protons trap NR1/NR2B NMDA receptors in a nonconducting state. *J Neurosci* **25**, 42–51 (2005).
31. Wyllie, D. J., Behe, P. & Colquhoun, D. Single-channel activations and concentration jumps: comparison of recombinant NR1a/NR2A and NR1a/NR2D NMDA receptors. *J Physiol* **510** (Pt 1), 1–18 (1998).
32. Umehiya, M., Senda, M. & Murphy, T. H. Behaviour of NMDA and AMPA receptor-mediated miniature EPSCs at rat cortical neuron synapses identified by calcium imaging. *J Physiol* **521** Pt 1, 113–122 (1999).
33. Nagy, G. G., Watanabe, M., Fukaya, M. & Todd, A. J. Synaptic distribution of the NR1, NR2A and NR2B subunits of the N-methyl-d-aspartate receptor in the rat lumbar spinal cord revealed with an antigen-unmasking technique. *Eur J Neurosci* **20**, 3301–3311 (2004).
34. Hatton, C. J. & Paoletti, P. Modulation of trimeric NMDA receptors by N-terminal domain ligands. *Neuron* **46**, 261–274 (2005).
35. Rauner, C. & Kohr, G. Triheteromeric NR1/NR2A/NR2B receptors constitute the major N-methyl-D-aspartate receptor population in adult hippocampal synapses. *J Biol Chem* **286**, 7558–7566 (2011).
36. Tovar, K. R., McGinley, M. J. & Westbrook, G. L. Triheteromeric NMDA Receptors at Hippocampal Synapses. *J Neurosci* **33**, 9150–9160 (2013).
37. Vance, K. M., Hansen, K. B. & Traynelis, S. F. GluN1 splice variant control of GluN1/GluN2D NMDA receptors. *J Physiol* **590**, 3857–3875 (2012).
38. Hummel, M., Strassle, B., Miller, S., Kaftan, E. & Whiteside, G. Anatomical localization and expression pattern for the NMDA-2D receptor subunit in a rat model of neuropathic pain. *Neuroscience* **155**, 492–502 (2008).
39. Jones, S. & Gibb, A. J. Functional NR2B- and NR2D-containing NMDA receptor channels in rat substantia nigra dopaminergic neurones. *J Physiol* **569**, 209–221 (2005).
40. Momiyama, A., Feldmeyer, D. & Cull-Candy, S. G. Identification of a native low-conductance NMDA channel with reduced sensitivity to Mg²⁺ in rat central neurones. *J Physiol* **494** (Pt 2), 479–492 (1996).
41. Brickley, S. G., Misra, C., Mok, M. H., Mishina, M. & Cull-Candy, S. G. NR2B and NR2D subunits coassemble in cerebellar Golgi cells to form a distinct NMDA receptor subtype restricted to extrasynaptic sites. *J Neurosci* **23**, 4958–4966 (2003).
42. Misra, C., Brickley, S. G., Farrant, M. & Cull-Candy, S. G. Identification of subunits contributing to synaptic and extrasynaptic NMDA receptors in Golgi cells of the rat cerebellum. *J Physiol* **524** Pt 1, 147–162 (2000).
43. Misra, C., Brickley, S. G., Wyllie, D. J. & Cull-Candy, S. G. Slow deactivation kinetics of NMDA receptors containing NR1 and NR2D subunits in rat cerebellar Purkinje cells. *J Physiol* **525** Pt 2, 299–305 (2000).
44. Harney, S. C., Jane, D. E. & Anwyl, R. Extrasynaptic NR2D-containing NMDARs are recruited to the synapse during LTP of NMDAR-EPSCs. *J Neurosci* **28**, 11685–11694 (2008).
45. Logan, S. M., Partridge, J. G., Matta, J. A., Buonanno, A. & Vicini, S. Long-lasting NMDA receptor-mediated EPSCs in mouse striatal medium spiny neurons. *J Neurophysiol* **98**, 2693–2704 (2007).
46. Brothwell, S. L. *et al.* NR2B- and NR2D-containing synaptic NMDA receptors in developing rat substantia nigra pars compacta dopaminergic neurones. *J Physiol* **586**, 739–750 (2008).
47. Harney, S. C. & Anwyl, R. Plasticity of NMDA receptor-mediated excitatory postsynaptic currents at perforant path inputs to dendrite-targeting interneurons. *The Journal of physiology* **590**, 3771–3786 (2012).
48. Volianskis, A. *et al.* Different NMDA receptor subtypes mediate induction of long-term potentiation and two forms of short-term potentiation at CA1 synapses in rat hippocampus in vitro. *J Physiol* **591**, 955–972 (2013).
49. Dunah, A. W., Luo, J., Wang, Y. H., Yasuda, R. P. & Wolfe, B. B. Subunit composition of N-methyl-D-aspartate receptors in the central nervous system that contain the NR2D subunit. *Mol Pharm* **53**, 429–437 (1998).
50. Pina-Crespo, J. C. & Gibb, A. J. Subtypes of NMDA receptors in new-born rat hippocampal granule cells. *J Physiol* **541**, 41–64 (2002).
51. Tong, C. K., Kaftan, E. J. & Macdermott, A. B. Functional identification of NR2 subunits contributing to NMDA receptors on substance P receptor-expressing dorsal horn neurons. *Mol Pain* **4**, 44 (2008).
52. Shiokawa, H., Kaftan, E. J., MacDermott, A. B. & Tong, C. K. NR2 subunits and NMDA receptors on lamina II inhibitory and excitatory interneurons of the mouse dorsal horn. *Mol Pain* **6**, 26 (2010).
53. Momiyama, A. Distinct synaptic and extrasynaptic NMDA receptors identified in dorsal horn neurones of the adult rat spinal cord. *J Physiol* **523** Pt 3, 621–628 (2000).
54. Wyllie, D. J., Behe, P., Nassar, M., Schoepfer, R. & Colquhoun, D. Single-channel currents from recombinant NMDA NR1a/NR2D receptors expressed in *Xenopus* oocytes. *Proc Biol Sci* **263**, 1079–1086 (1996).
55. Cho, K. K., Khibnik, L., Philpot, B. D. & Bear, M. F. The ratio of NR2A/B NMDA receptor subunits determines the qualities of ocular dominance plasticity in visual cortex. *Proc Natl Acad Sci U S A* **106**, 5377–5382 (2009).
56. MacDonald, J. F., Jackson, M. F. & Beazely, M. A. Hippocampal long-term synaptic plasticity and signal amplification of NMDA receptors. *Crit Rev Neurobiol* **18**, 71–84 (2006).
57. Woolf, C. J. Windup and central sensitization are not equivalent. *Pain* **66**, 105–108 (1996).
58. Hildebrand, M. E. *et al.* Identification of sodium channel isoforms that mediate action potential firing in lamina I/II spinal cord neurons. *Mol Pain* **7**, 67 (2011).
59. Chery, N., Yu, X. H. & de Koninck, Y. Visualization of lamina I of the dorsal horn in live adult rat spinal cord slices. *J Neurosci Methods* **96**, 133–142 (2000).
60. Molander, C., Xu, Q. & Grant, G. The cytoarchitectonic organization of the spinal cord in the rat. I. The lower thoracic and lumbosacral cord. *J Comp Neurol* **230**, 133–141 (1984).
61. McNeill, D. L., Coggeshall, R. E. & Carlton, S. M. A light and electron microscopic study of calcitonin gene-related peptide in the spinal cord of the rat. *Exp Neurol* **99**, 699–708 (1988).
62. Lima, D. & Coimbra, A. A Golgi study of the neuronal population of the marginal zone (lamina I) of the rat spinal cord. *J Comp Neurol* **244**, 53–71 (1986).
63. Prescott, S. A. & De Koninck, Y. Four cell types with distinctive membrane properties and morphologies in lamina I of the spinal dorsal horn of the adult rat. *J Physiol* **539**, 817–836 (2002).
64. Singh, A., Hildebrand, M. E., Garcia, E. & Snutch, T. P. The transient receptor potential channel antagonist SKF96365 is a potent blocker of low-voltage-activated T-type calcium channels. *Br J Pharmacol* **160**, 1464–1475 (2010).
65. McGale, E. H., Pye, I. F., Stonier, C., Hutchinson, E. C. & Aber, G. M. Studies of the inter-relationship between cerebrospinal fluid and plasma amino acid concentrations in normal individuals. *J Neurochem* **29**, 291–297 (1977).
66. Ahmadi, S. *et al.* Facilitation of spinal NMDA receptor currents by spillover of synaptically released glycine. *Science* **300**, 2094–2097 (2003).
67. Berger, A. J., Dieudonne, S. & Ascher, P. Glycine uptake governs glycine site occupancy at NMDA receptors of excitatory synapses. *J Neurophysiol* **80**, 3336–3340 (1998).
68. Bergeron, R., Meyer, T. M., Coyle, J. T. & Greene, R. W. Modulation of N-methyl-D-aspartate receptor function by glycine transport. *Proc Natl Acad Sci U S A* **95**, 15730–15734 (1998).

Acknowledgments

This study was supported by a grant from the Canadian Institutes of Health Research (CIHR) to MWS (MT-12682). MWS holds a Tier 1 Canada Research Chair in Neuroplasticity and Pain, and is the Anne and Max Tanenbaum Chair in Molecular Medicine at the Hospital for Sick Children. MEH was supported by a postdoctoral fellowship from CIHR and MEH and EH were supported by Pain Scientist Awards from the University of Toronto Centre for the Study of Pain.

Author contributions

M.E.H., G.M.P., E.K.H., H.L. and S.B. contributed to data acquisition and analysis. M.E.H. designed, performed and analyzed whole-cell experiments for mEPSCs. E.K.H. performed and analyzed imaging experiments and performed some mEPSC experiments. G.M.P. performed and analyzed whole-cell experiments for unitary synaptic currents. M.W.S. conceptualized and supervised the project and contributed to the design of the experiments. M.E.H., G.M.P. and M.W.S. wrote the main manuscript. All authors reviewed the manuscript.

Additional information

Supplementary information accompanies this paper at <http://www.nature.com/scientificreports>



Competing financial interests: The authors declare no competing financial interests.

How to cite this article: Hildebrand, M.E. *et al.* GluN2B and GluN2D NMDARs dominate synaptic responses in the adult spinal cord. *Sci. Rep.* **4**, 4094; DOI:10.1038/srep04094 (2014).



This work is licensed under a Creative Commons Attribution-NonCommercial-ShareAlike 3.0 Unported license. To view a copy of this license, visit <http://creativecommons.org/licenses/by-nc-sa/3.0>